Supplemental Material can be found at:
http://www.jbc.org/content/suppl/2012/02/07/M111.324525.DC1.html

THE JOURNAL OF BIOLOGICAL CHEMISTRY VOL. 287, NO. 14, pp. 11252–11260, March 30, 2012
© 2012 by The American Society for Biochemistry and Molecular Biology, Inc. Published in the U.S.A.

Kinetics of Precursor Interactions with the Bacterial Tat Translocase Detected by Real-time FRET*[S]

Received for publication, November 15, 2011, and in revised form, February 2, 2012 Published, JBC Papers in Press, February 7, 2012, DOI 10.1074/jbc.M111.324525

Neal Whitaker, Umesh K. Bageshwar, and Siegfried M. Musser[1]

From the Department of Molecular and Cellular Medicine, College of Medicine, The Texas A&M Health Science Center, 1114 TAMU, College Station, Texas 77843

Background: The Tat machinery transports folded proteins from the bacterial cytoplasm to the periplasm.
Results: A $\Delta\psi$ is required for a Tat cargo to move away from the TatBC receptor complex.
Conclusion: Cargo migration away from the TatBC complex requires a $\Delta\psi$-dependent assembly step or conformational change.
Significance: Cargo migration from the TatBC receptor is a major rate-limiting step of Tat transport.

The *Escherichia coli* twin-arginine translocation (Tat) system transports fully folded and assembled proteins across the inner membrane into the periplasmic space. Traditionally, *in vitro* protein translocation studies have been performed using gel-based transport assays. This technique suffers from low time resolution, and often, an inability to distinguish between different steps in a continuously occurring translocation process. To address these limitations, we have developed an *in vitro* FRET-based assay that reports on an early step in the Tat translocation process in real-time. The natural Tat substrate pre-SufI was labeled with Alexa532 (donor), and the fluorescent protein mCherry (acceptor) was fused to the C terminus of TatB or TatC. The colored Tat proteins were easily visible during purification, enabling identification of a highly active inverted membrane vesicle (IMV) fraction yielding transport rates with NADH almost an order of magnitude faster than previously reported. When pre-SufI was bound to the translocon, FRET was observed for both Tat proteins. FRET was diminished upon addition of nonfluorescent pre-SufI, indicating that the initial binding step is reversible. When the membranes were energized with NADH, the FRET signal was lost after a short delay. These data suggest a model in which a Tat cargo initially associates with the TatBC complex, and an electric field gradient is required for the cargo to proceed to the next stage of transport. This cargo migration away from the TatBC complex requires a significant fraction of the total transport time.

The bacterial twin-arginine translocation (Tat)[2] machinery transports protein cargos from the cytoplasm to the periplasm (1, 2). A functional *Escherichia coli* Tat machinery minimally consists of three membrane proteins, TatA (or TatE), TatB, and TatC (3–7). TatB and TatC are expressed at approximately equal levels (8), and together act as the receptor for precursor proteins (9, 10). TatA is expressed at higher levels than TatB and TatC (8), and can form ring-like structures *in vitro* (11). A popular model is that cargos are first recruited by TatBC complexes, and are then conveyed across the membrane by a protein conducting channel comprised of TatA oligomers (11, 12). After transport, Tat signal peptides are cleaved from precursor proteins by the LepB peptidase (13, 14). Recent studies have suggested that precursor binding to the cytoplasmic face of the inner membrane is a functional intermediate in the transport process (15, 16). A proton motive force (PMF) is essential for translocon assembly and cargo transport (17–19). In *E. coli*, only the membrane potential ($\Delta\psi$) component of the PMF is required for transport (20).

Both TatB and TatC participate in binding and recognition of signal peptides. Bacterial Tat signal peptides contain an (S/T)RR*X*FLK consensus motif, a hydrophobic domain, and a short polar domain which precedes the signal sequence cleavage site (21–23). Based on mutant suppression, alanine substitutions and cross-linking experiments, the N-terminal half of TatC interacts with the twin-arginine portion of the signal peptide (24–27). Cross-linking indicates that TatB interacts with the C-terminal end of the signal peptide (24, 27). TatB also makes extensive contacts with the cargo mature domain, presumably through its cytoplasmic domain (28).

It is unclear how the cargo proceeds across the membrane after recognition by the TatBC complex. A severe constraint on possible models is the finding that the mature domain can be efficiently translocated when the signal sequence is cross-linked to TatC near the twin-arginine motif (27). One possibility is that TatA somehow assists with flipping the mature domain from one side of the membrane to the other while the signal sequence remains tethered (27). In this picture, the signal peptide may initially only partially occupy a transmembrane binding pocket before transport, and full binding only occurs during or after transport, consistent with the identification of deep insertion of the signal peptide and distinct translocation intermediates (29–31). Electron microscopic images of purified TatBC complexes revealed cargo bound within the membrane plane, possibly reflecting cargo in transit (32).

Fluorescence resonance energy transfer (FRET) can provide time-dependent distance information at low protein concentrations. Here we report the use of FRET to probe the binding of

* This work was supported, in whole or in part, by National Institutes of Health Grant R01 GM065534 (to S. M. M.).
[S] This article contains supplemental Figs. S1–S11.
[1] To whom correspondence should be addressed: Department of Molecular and Cellular Medicine, College of Medicine, The Texas A&M Health Science Center, 1114 TAMU, College Station, TX 77843. Tel.: 979-862-4128; Fax: 979-847-9481; E-mail: smusser@tamu.edu.
[2] The abbreviations used are: Tat, twin-arginine translocation; FRET, fluorescence resonance energy transfer; IMV, inverted membrane vesicle.

Downloaded from www.jbc.org at Texas A&M University - Medical Sciences Library, on April 2, 2012

a cargo to the TatBC complex, and its migration away from this complex, either by dissociation or by movement along the transport pathway. We found that the TatBC complex has a nanomolar affinity for pre-SufI, and that an electric field gradient is required for migration beyond the initial binding step.

EXPERIMENTAL PROCEDURES

Bacterial Strains, Plasmids, and Growth Conditions—*E. coli* strains MC4100ΔTatABCDE, JM109, and BL21(λDE3) were described previously (33–36). Cultures for IMV preparations were grown at 37 °C as described (20). Overexpression cultures for pre-SufI and spTorA-mCherry-MA were grown in Luria-Bertani (LB) medium at 37 °C, and shifted to 15 °C upon induction with 1 mM IPTG or 0.6% arabinose, respectively. All cultures were supplemented with ampicillin (50 μg/ml). Tat proteins were induced for 4 h with 0.7% arabinose, as previously described (20).

The plasmid pIntein-preSufI-MA was generated by inserting a cysteine-free form of pre-SufI with a 6×His tag into the vector pTYB11 (New England Biochem). Plasmid pIntein-pre-SufI-MA was used as the template for all pre-SufI mutants, as described in supplemental Fig. S1. Plasmids pTatAB^{cherry}C and pTatABC^{cherry} were generated by insertion of the mCherry sequence (plasmid pmCherry, Clontech) into pTatABC (13) immediately after the coding regions of TatB and TatC, respectively (supplemental Figs. S2 and S3). pTatBC and pTatBC^{cherry} were generated by excising the TatA sequence from pTatABC and pTatABC^{cherry}, respectively (supplemental Fig. S4). All mutations were generated via the Quikchange protocol (Stratagene), and all plasmid coding sequences were verified by DNA sequencing. Plasmid pTorA-mCherry-H6 was generated by inserting mCherry along with the TorA signal peptide and 4 amino acids (AQAA) of the TorA mature domain into the pBAD24 vector (supplemental Fig. S5).

Protein Purification and Labeling—All pre-SufI proteins were purified from expression cultures via chitin chromatography as described previously (37) with an on-column cleavage (50 mM dithiothreitol) at 4 °C for 20 h (supplemental Fig. S6). Excess dithiothreitol was removed from the eluate by dialysis (10,000 MW cutoff) against phosphate-buffered saline (1× PBS: 137 mM NaCl, 2.7 mM KCl, 10 mM Na_2HPO_4, and 2 mM KH_2PO_4, pH 7.5) for 4 h. Ni-NTA chromatography was used for further purification (20). Alexa532 labeling of pre-SufI proteins was performed as described previously (15). After a 4 h dialysis against 1× PBS buffer, excess dye was removed by an additional Ni-NTA purification step (15). The final storage buffer was 20 mM Tris-HCl, 50 mM NaCl, 250 mM imidazole, 50% glycerol, pH 8.0. Purification of spTorA-mCherry-H6 was performed by Ni-NTA chromatography, by the procedure used for pre-SufI (20). The mCherry protein was obtained by purifying the mature protein from a spTorA-mCherry-H6 preparation via Resource Q (GE Healthcare) chromatography.

The protein concentrations of all pre-SufI proteins were quantified by SDS-PAGE using bovine serum albumin as the standard. Spot intensities after Coomassie Blue staining were determined with a phosphorimager (model FX PhosphoImager, Bio-Rad). Alexa532 concentrations were determined by absorbance spectroscopy at 532 nm (ϵ = 81,000 cm^{-1} M^{-1}). Typical dye-to-protein ratios after labeling indicated that 80–90% of the cysteines were successfully tagged. mCherry concentrations were estimated in 2% SDS based on the mCherry absorbance at 587 nm and its extinction coefficient at this wavelength (38).

Isolation of IMVs—IMVs were isolated from MC4100ΔTatABCDE as described (20), with the following modifications. Cell lysis by French press was performed at ~16,000 psi instead of ~6,000 psi. In addition, the 2.3 M sucrose cushion was replaced with a 3-step (0.5, 1.5, and 2.3 M) sucrose gradient, which enabled enrichment of a highly active inner membrane fraction. A band in the 0.5 M region was faintly pink when mCherry Tat fusions were expressed (supplemental Fig. S7), and translucent dark brown when wild type TatABC was expressed. IMV concentrations were determined as the A_{280} in 2% SDS (20).

Transport and Membrane Binding Assays—*In vitro* transport assays and precursor-membrane binding assays were performed as described (15, 20), unless otherwise indicated. Gel-based transport kinetics were performed in a heated cuvette to mimic conditions in which the real-time FRET assays were performed. Aliquots (35 μl) of the reaction mixture were removed from the cuvette at the indicated time points and quenched with a mixture of 5 μM nigericin and 5 μM valinomycin on ice. Visualization of protein bands was performed by direct in-gel fluorescence imaging (model FX PhosphorImager, Bio-Rad).

Real-time FRET Assay—Translocation buffer (5 mM $MgCl_2$, 50 mM KCl, 200 mM sucrose, 57 μg ml^{-1} BSA, 25 mM MOPS, 25 mM MES, pH 8.0) (20) and IMVs (A_{280} = 2) were added to a heated cuvette (final volume: 800 μl) in an SLM-Aminco fluorometer and allowed to equilibrate to 37 °C for 5 min. Precursor protein was then added, and equilibration was continued for at least 200 s. Reactions were initiated by addition of competitor precursor or NADH. Excitation and emission wavelengths were 500 nm (4 nm slits) and 550 nm (8 nm slits), respectively.

Analysis—Kinetic data were fit with a single exponential plus a linear baseline drift,

$$y = ax + b(1 - e^{-kx}) \quad \text{(Eq. 1)}$$

where a, b, and k (= $1/\tau$) are fit parameters. The data in Fig. 2*D* were fit to the equation for single site binding when the K_D and receptor concentration are of similar magnitude (derived in the supplemental materials),

$$y = C^* \frac{(x + T_0 + K_D) - \sqrt{(x + T_0 + K_D)^2 + 4(x)T_0}}{2T_0} \quad \text{(Eq. 2)}$$

where C, T_0, and K_D are fit parameters.

RESULTS

Experimental Design—Our goal was to examine the interaction between the TatBC receptor complex and a cargo under real-time transport conditions. To this end, we used FRET, with a donor fluorophore (Alexa532) on the cargo and an acceptor fluorophore (mCherry) on one of the Tat proteins. We assumed that binding would result in a decrease in donor fluorescence due to FRET. The fluorescent cargo selected was the natural Tat substrate pre-SufI. Eight different single cysteine mutants of

Downloaded from www.jbc.org at Texas A&M University - Medical Sciences Library, on April 2, 2012

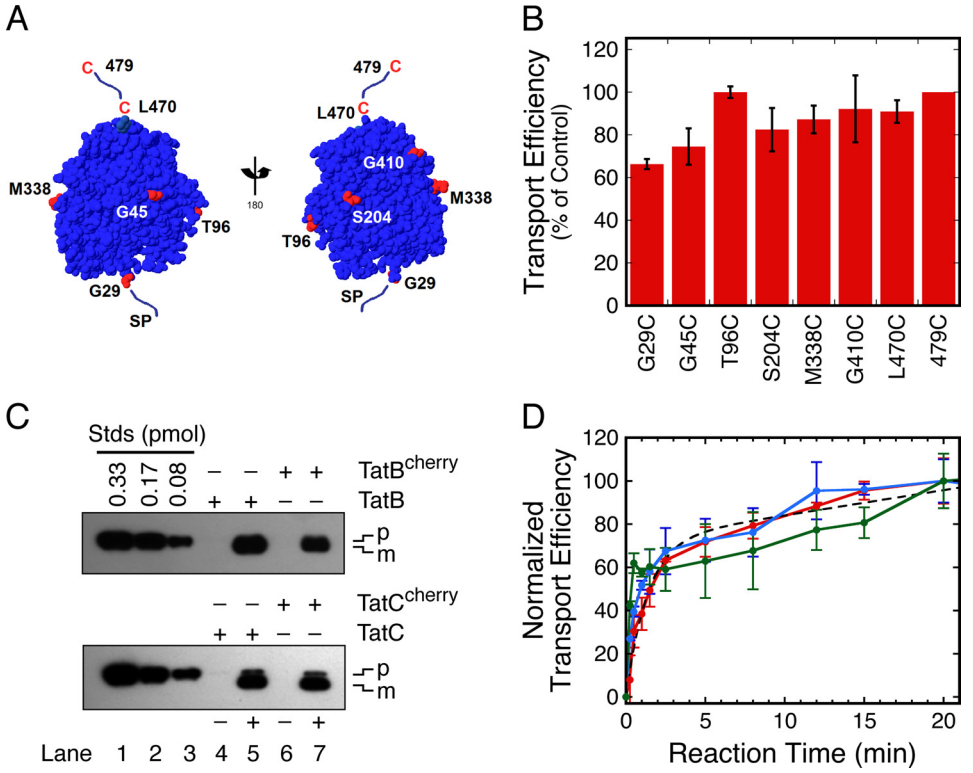

FIGURE 1. **Pre-SufI cysteine mutants and influence of TatB^{cherry} and TatC^{cherry} on Tat transport.** *A*, location of single cysteine mutations. Residues mutated to cysteine are indicated in *red* (PDB accession number: 2UXT). Cysteines were labeled with Alexa532 maleimide for transport and FRET experiments. *B*, transport efficiencies of Alexa532 labeled pre-SufI mutants. Transport reactions (30 min) were performed with TatABC IMVs (A_{280} = 5), 4 mM NADH and 90 nM pre-SufI. Transport efficiencies were normalized to the 479C mutant (n = 3). *C*, transport of pre-SufI(479C)^{Alexa532} into IMVs containing TatAB^{cherry}C, TatABC^{cherry} or wt TatABC. Transport requires NADH to generate the necessary $\Delta\psi$. The mCherry domain has no apparent effect on transport efficiency. *Lanes 1–3* are pre-SufI concentration standards. The location of precursor (*p*) and mature (*m*) molecular weight bands are identified. Conditions are the same as in *B*. *D*, kinetics of pre-SufI(479C)^{Alexa532} (20 nM) transport into IMVs (A_{280} = 2) containing wt TatABC (*blue*), TatAB^{cherry}C (*green*), and TatABC^{cherry} (*red*). Transport efficiencies were normalized based on the 20 min time point. The *black dashed curve* is a single exponential plus linear baseline fit to the TatABC^{cherry} data (τ = 81 s).

pre-SufI were generated. The different cysteine mutations were spread over the surface of the protein (Fig. 1A). These mutants were labeled with Alexa532 maleimide. The C-terminal cysteine mutant, pre-SufI(479C), serves as our wild type (wt) reference because previous experiments indicated that a C-terminal dye had no effect on transport efficiency (15). The T96C and 479C mutants yielded the highest transport efficiencies (Fig. 1*B*).

To exclude any endogenous (and therefore unlabeled) Tat proteins from IMV preparations, TatB^{cherry} and TatC^{cherry} were expressed in the Tat deletion strain MC4100ΔTatABCDE. The mCherry domain did not significantly affect transport efficiency (Fig. 1*C*) or transport kinetics (Fig. 1*D*). The fluorescent TatB and TatC proteins allowed us to visually monitor the IMV purification process. Consequently, we identified a minor membrane-containing band within the 0.5 M sucrose region of the sucrose gradient that had the majority of the mCherry protein (supplemental Fig. S7). The MC4100 membranes recovered from this band catalyzed pre-SufI transport about an order of magnitude faster (Fig. 1*D*) than reported previously for JM109 IMVs (15, 20). Further, IMVs prepared with our current protocol were more consistently active. Previously, we were not able to consistently obtain active membranes from MC4100 (20).

The FRET Signal—IMVs isolated from *E. coli* expressing TatAB^{cherry}C or TatABC^{cherry} exhibited two fluorescence peaks at ~610 nm and ~641 nm (supplemental Fig. S8, *A* and *B*). These peaks both arise from mCherry (supplemental Fig. S8*C*). Addition of pre-SufI^{Alexa532} resulted in a third peak at ~550 nm (Fig. 2*A*). The decrease in donor fluorescence signal due to FRET was most easily verified by addition of a competitor protein (non-fluorescent cargo), which resulted in an increase in the 550 nm peak, presumably due to replacement of the bound fluorescent protein with the non-fluorescent competitor (Fig. 2*A*). No increase in 550 nm emission was observed upon competitor addition if mCherry was not attached to the Tat proteins (supplemental Fig. S8*D*), indicating that the decrease in 550 nm emission when the fluorescent cargo was bound to the Tat translocon (Fig. 2*A*) was indeed due to FRET. The strong mCherry fluorescence emission far from the excitation wavelength of 500 nm indicates a high concentration relative to the cargo. The mCherry concentration was estimated as 322 ± 88 nM (n = 5) under typical assay conditions, over an order of magnitude higher than the pre-SufI concentration of 20 nM (Fig. 2*A*). These values are consistent with the amounts of pre-SufI^{Alexa532} and mCherry needed to approximately reproduce the emission spectra in Fig. 2*A* in an IMV-free mixture (supplemental Fig. S8*D*). Any increase in mCherry emission due to FRET was weak and not reliably detected. This is expected if the mCherry acceptor molecules self-quench due to their proximity in a TatBC oligomer (32).

Downloaded from www.jbc.org at Texas A&M University - Medical Sciences Library, on April 2, 2012

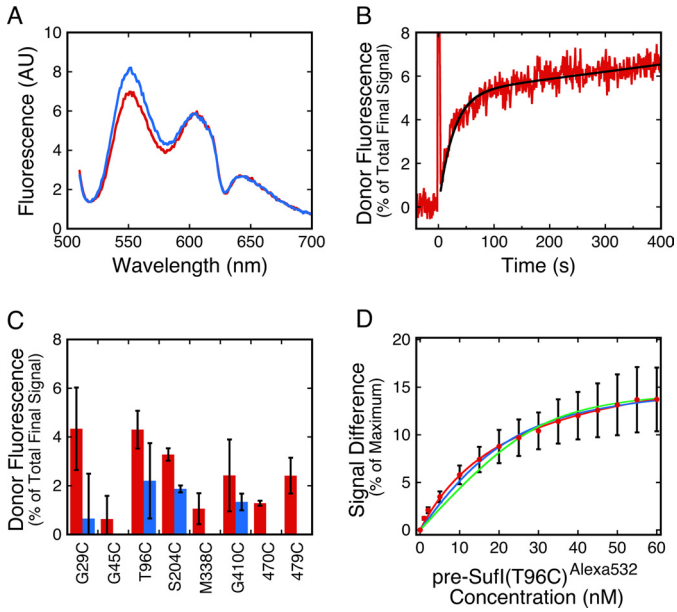

FIGURE 2. **FRET between the pre-SufI cargo and the Tat translocon.** *A*, emission scan (EX = 500 nm) of pre-SufI(T96C)^{Alexa532} (20 nM) and TatABC^{cherry} IMVs (A_{280} = 2) before (*red*) and after (*blue*) addition of 200 nM unlabeled pre-SufI(T96C). The increase in signal at 550 nm indicates loss of FRET. The overall signal change is not a good measure of FRET efficiency since a high fraction of the cargo is not bound to Tat translocons (*i.e.* free in solution or bound to the lipids). *B*, time trace of the fluorescence emission at 550 nm (donor) for the experiment in *A*. Unlabeled pre-SufI(T96C) was added at t = 0 s. The competitor-induced loss of FRET occurred with a time constant of 24 ± 2 s (n = 3). *C*, total FRET signal observed for various pre-SufI mutants, determined as in *B*. IMVs contained TatABC^{cherry} (*red*) or TatAB^{cherry}C (*blue*) (n = 3). The absence of *blue bars* for some mutants indicates no FRET to TatB^{cherry}. *D*, precursor binding affinity and receptor concentration estimated from the concentration dependence of the FRET signal. TatABC^{cherry} IMVs were titrated with pre-SufI(T96C)^{Alexa532} in the presence and absence of 300 nM unlabeled pre-SufI(T96C). Shown here is the average difference (n = 5) between two titration curves, such as those shown in supplemental Fig. S10. Three fits are shown in which the receptor concentration (T_0) was fixed and the K_D and maximum signal were fitting parameters: (*red*) T_0 = 0.1 nM, K_D = 23 nM; (*blue*) T_0 = 20 nM, K_D = 7.5 nM; (*green*) T_0 = 30 nM, K_D = 3.6 nM. These fits indicate that $T_0 \approx$ 0–20 nM and $K_D \approx$ 7–23 nM. Details of the analysis are described in the supplemental materials.

Maximizing the FRET Efficiency—Having determined that FRET indeed occurred upon binding of the cargo to the Tat translocon, we next sought to maximize the FRET signal. This was accomplished by individually attaching the donor dye to the 8 locations identified in Fig. 1*A*, which cover the surface of pre-SufI. In addition, the mCherry acceptor was attached to either TatB or TatC. FRET signal intensity was determined from kinetic experiments in which non-fluorescent competitor cargo was added to IMVs with prebound fluorescent cargo (Fig. 2*B*). For pre-SufI(T96C), the competitor released the bound cargo with τ = 24 ± 2 s (Fig. 2*B*). Control kinetic experiments in the absence of a donor or acceptor fluorophore confirmed the transient FRET signal (supplemental Fig. S9*A*). We found that TatC^{cherry} yielded stronger FRET signals than TatB^{cherry} (Fig. 2*C*). Two pre-SufI mutants, G29C and T96C, yielded similarly strong FRET signals when the mCherry domain was attached to TatC (Fig. 2*C*). However, labeling at G29C reduced transport efficiency (Fig. 1*B*). To convert the relative FRET signals into reliable distance and/or orientation information, the data in Fig. 2*C* need to be corrected based on binding affinity. We attempted to do this using our previous binding assay (15), but the errors of these binding measurements and the errors of the FRET measurements were too high to provide meaningful information. Instead, we settled on using TatC^{cherry} and the T96C mutant of pre-SufI for all subsequent experiments since these proteins yielded the strongest FRET signal while retaining transport efficiency (Figs. 1*B* and 2*C*).

Binding Affinity—The FRET signal was used to estimate the cargo-TatBC binding affinity. Two titrations were done. The first titration involved adding increasing amounts of fluorescent pre-SufI(T96C) to IMVs. The second titration was identical to the first, except that a large excess of non-fluorescent cargo was preincubated with the IMVs (supplemental Fig. S10). The difference in donor fluorescence intensity between the two titrations (FRET signal) reflects the amount of fluorescent cargo bound to the translocon (Fig. 2*D*). Based on the mCherry concentration, the Tat receptor concentration is high relative to the apparent K_D. Thus, the data in Fig. 2*D* were fit with Equation 2 ("Experimental Procedures" and supplemental materials), which explicitly includes the receptor concentration as a fit parameter. Unfortunately, the receptor concentration and K_D are not uniquely determined from the data. However, the data indicate that the functional receptor concentration is $\leq \sim$20 nM and the $K_D \approx$ 7–23 nM (see Fig. 2*D* and supplemental materials for a detailed explanation).

FRET Decreases upon Membrane Energization—When fluorescent pre-SufI was prebound to IMVs containing Tat-mCherry fusions and the membranes were subsequently energized by the addition of NADH, the donor fluorescence signal increased (a decrease in FRET). This was observed for membranes containing either TatB^{cherry} or TatC^{cherry} (Fig. 3*A*). Control experiments in the absence of donor or acceptor fluorophore confirmed the NADH-dependent loss of FRET (supplemental Fig. S9*B*). Since NADH addition initiates transport across the membrane, these data are consistent with migration of the cargo away from its initial binding site on the TatBC complex as part of the transport process. It is unclear if the observed kinetics reflect migration elsewhere within the translocon (*e.g.* to the TatA pore) or immediate movement across the membrane. NADH generates a PMF, which is necessary for Tat transport. It was shown earlier that the $\Delta\psi$ and not the ΔpH component of the PMF is essential for Tat transport (20). We therefore tested whether the observed FRET signal is sensitive to these two PMF components. We found that the decrease in FRET upon NADH addition requires a $\Delta\psi$ and not a ΔpH (Fig. 3*B*), consistent with the hypothesis that the observed changes in the FRET signal report a transport substep.

A $\Delta\psi$-dependent Step Precedes Cargo Migration Away from the TatBC Complex—Exponential NADH-dependent FRET changes (τ = $\sim$30 s) were preceded by a lag phase (Fig. 3*A*). The duration of the delay was dependent on the batch of IMVs (*e.g.* compare Fig. 3, *A* and *B*), and ranged from $\sim$20 to $\sim$45 s (n = 9). This delay did not arise from slow formation of the $\Delta\psi$, as the $\Delta\psi$ forms within seconds (Fig. 3*C*). While it takes $\sim$25–30 s for the ΔpH to become fully established (Fig. 3*C*), it was shown earlier (20) and here (Fig. 3*B*) that the ΔpH is not necessary for transport. Therefore, the slow formation of the ΔpH does not explain the lag phase. Consequently, we reasoned that the lag phase could be explained by a $\Delta\psi$-dependent conformational

Downloaded from www.jbc.org at Texas A&M University - Medical Sciences Library, on April 2, 2012

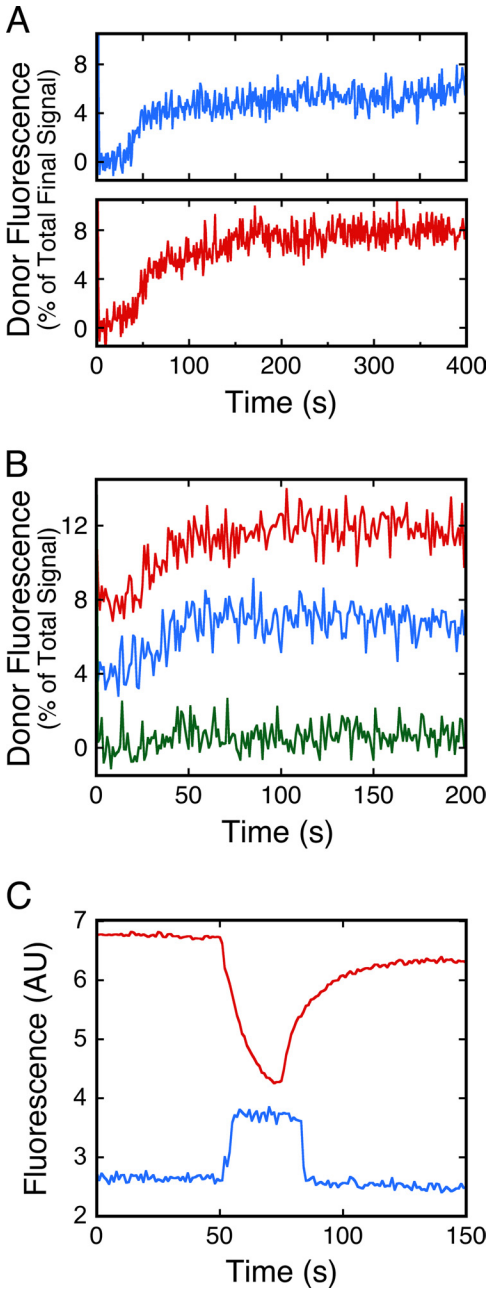

FIGURE 3. **Effect of PMF components on the FRET signal.** *A*, time trace of the fluorescence emission at 550 nm (donor) upon membrane energization. Reactions contained pre-SufI(T96C)^{Alexa532} (20 nM) and IMVs (A_{280} = 2) with TatAB^{cherry}C (*blue*) or TatABC^{cherry} (*red*). NADH (4 mM) was added at t = 0 s. *B*, sensitivity of NADH-dependent fluorescence changes to components of the PMF. The ΔpH and Δψ were reduced with nigericin (5 μM, *blue*) and valinomycin (5 μM, *green*), respectively. The control trace (*red*) contains no ionophores. Conditions as in *A* with TatABC^{cherry} IMVs (n = 2). *C*, gradients across membranes of TatABC^{cherry} IMVs (A_{280} = 2). The presence of Δψ (*blue*) and ΔpH (*red*) gradients were determined using 100 nM oxonol VI (EX = 610 nm, EM = 645 nm) and 2.5 μM quinacrine (EX = 420 nm, EM = 510 nm), respectively, as described previously (15). NADH (4 mM) was added at t = 50 s.

change or oligomerization process that is required for the cargo to migrate away from the TatBC binding site. We tested this hypothesis by preincubating the IMVs with NADH and then adding the cargo after a short delay (Fig. 4). The lag phase largely disappeared when the cargo was added 200 s after NADH (Fig. 4*C*). Under these conditions, slower kinetics (τ = ~70–90 s) were observed.

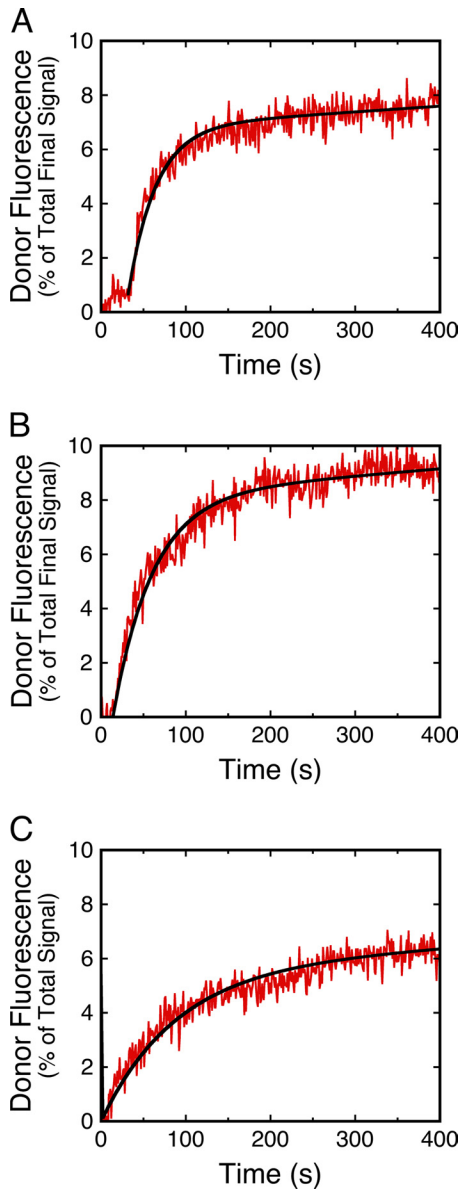

FIGURE 4. **Cargo migration kinetics depend on the interval between energization and cargo addition times.** The time-dependent donor fluorescence emission (550 nm) was measured for transport reactions containing TatABC^{cherry} IMVs (A_{280} = 2) and pre-SufI(T96C)^{Alexa532} (20 nM). Membranes were energized with NADH (4 mM) and the cargo was added 0 s (*A*), 10 s (*B*), or 200 s (*C*) later. Cargo was added at t = 0 s. The kinetics after the lag phase in *A* and *B* were fit with a single exponential plus a linear baseline drift ("Experimental Procedures"), yielding τ = 33 s and 46 s, respectively. The entire trace in *C* was fit with the same equation, yielding τ = 93 s. The linear baseline drift accounts for ~11% of the total fit fluorescence change for all three panels. Each trace represents an average of three individual runs.

Pre-SufI Is Released from TatBC Complexes when Membranes Are Energized in the Absence of TatA—As a control experiment for the NADH-dependent loss of FRET (Fig. 3*A*), we repeated these experiments in the absence of TatA. Similar levels of TatB and TatC^{cherry} were recovered in IMVs in the presence and absence of TatA (supplemental Fig. S11). Since TatA is required for transport, our expectation was that the cargo would remain bound to the TatBC complex, and hence, the FRET signal would remain constant. Experiments similar to those in Fig. 3*A* were performed, where pre-SufI was allowed to bind to IMVs, and NADH was added at time zero. FRET imme-

Downloaded from www.jbc.org at Texas A&M University - Medical Sciences Library, on April 2, 2012

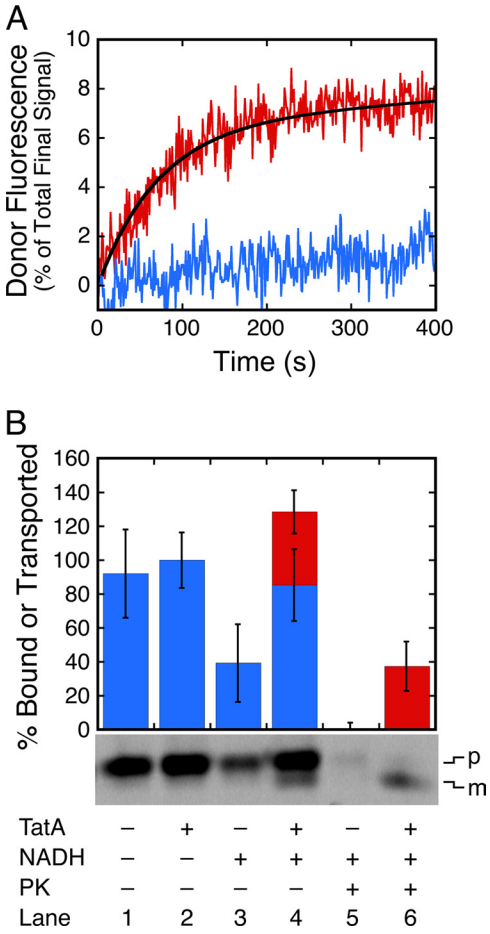

FIGURE 5. **Transport and binding to energized membranes in the absence of TatA.** *A*, time traces of donor emission (at 550 nm) in the presence or absence of mCherry after energization with 4 mM NADH at $t = 0$. Reactions contained pre-SufI(T96C)^{Alexa532} (20 nM) and IMVs with TatBC^{cherry} (*red*) or TatBC (*blue*) ($A_{280} = 2$). The TatBC^{cherry} data were fit with a single exponential plus a linear baseline drift, yielding $\tau = 71$ s (the baseline drift accounts for 13% of the total fluorescent change). *B*, membrane binding and cargo transport in the presence and absence of TatA. Pre-SufI(T96C)^{Alexa532} (20 nM) was allowed to bind to membranes (TatBC or TatABC IMVs, $A_{280} = 2$) for 10 min at 37 °C, respectively. After a 10 min binding period, control samples were then centrifuged (16,000 × *g*, 45 min, room temperature), and the pellet fractions were analyzed by SDS-PAGE (*lanes 1–2*). Resuspended membranes were energized with 4 mM NADH for 20 min at 37 °C (*lanes 3–6*). Proteinase K (PK, 0.7 mg/ml) was added to half the reactions and all reactions were immediately centrifuged (16,000 × *g*, 45 min, room temperature). The resultant membrane pellets were resuspended in translocation buffer containing 68 mM PMSF and resolved via SDS-PAGE. The amounts of recovered precursor (p, *blue*) and mature (m, *red*) proteins are shown above the sample gel, as indicated ($n = 3$). Less pre-SufI was recovered with membranes lacking TatA (compare *lanes 3* and *4*), indicating that the TatBC affinity for pre-SufI is lower without TatA in the presence of a PMF. Matured protein was protease protected (compare *lanes 4* and *6*), indicating transport. The average amount of protein initially recovered with TatABC membranes (*lane 2*) was set to 100%.

diately decreased ($\tau = 71$ s) when the membranes were energized in the absence of TatA (Fig. 5*A*). This differed from results obtained with IMVs containing TatA (Figs. 3*A* and 4*A*), which exhibited a lag-phase and rapid loss of FRET after the lag phase ($\tau = \sim 30$ s). Since the Tat machinery is incapable of transport without TatA (or its paralog, TatE) (5), the observed loss of FRET is not due to cargo translocation across the membrane, as confirmed in Fig. 5*B*. Rather, likely possibilities are that the loss of FRET arises either from a conformational change that results in the mature domain of the bound precursor moving away from the mCherry fluorophore, or from the precursor dissociating from the TatBC complex entirely. The latter appears to be the case since TatBC IMVs pelleted after energization retain ~53% less bound pre-SufI than unenergized IMVs (Fig. 5*B*). Multiple groups have suggested the possibility that the signal peptide can penetrate fairly deeply into the membrane (26, 29, 31, 39). The energy-dependent dissociation of pre-SufI from the receptor complex in the absence of TatA suggests the possibility that the signal sequence may not have penetrated as deeply under these conditions.

DISCUSSION

Tat transport requires both binding of a pre-protein to the Tat proteins as well as movement of the cargo across the membrane. Presumably, these two seemingly conflicting processes are coupled, i.e. the binding reaction gates the transport event. Critical to understanding this process is the development and analysis of assays that can identify and discern the conversion between substeps of transport. To this end, we developed a FRET assay that reports the initial cargo binding step. Our major conclusions are: 1) transport occurs on the minute timescale with a highly purified membrane fraction (Fig. 1*D*); 2) the cargo binding interaction occurs with an apparent $K_D \approx 7$–23 nM (Fig. 2*D*) and a competitor-induced $k_{off} \approx 0.042\ s^{-1}$ (=1/24 s) (Fig. 2*B*); 3) the cargo mature domain appears to be nearer to the C terminus of TatC than the C terminus of TatB (Fig. 2*C*); 4) migration of the cargo from its initial binding site requires a $\Delta\psi$ (Fig. 3*B*); 5) a delay in cargo migration from the initial binding site occurs after membrane energization (Figs. 3 and 4), indicating that the $\Delta\psi$ does not directly promote cargo migration; and 6) TatA increases the affinity of the TatBC receptor complex for the precursor in the presence of a membrane potential (Fig. 5). The implications of these results are now discussed.

As far as we are aware, the binding experiments reported here provide the first estimate of the binding affinity of a signal peptide for functional *E. coli* Tat translocons. The estimated K_D of 7–23 nM indicates a fairly strong, highly specific interaction, as is reasonably expected for a selective process. From this measured K_D and the competitor-induced $k_{off} \approx 0.042\ s^{-1}$ (Fig. 2*B*), the apparent k_{on} is 10^6-$10^7\ M^{-1}\ s^{-1}$. This second order rate constant is of the magnitude expected for enzymatic interactions, where orientation of the reactants is clearly important, and is complicated by the fact that it likely reflects both binding to the membrane lipids (15) as well as lateral diffusion to the Tat translocon. Whereas the precursor can apparently exchange between lipid- and translocon-bound forms on the tens of seconds timescale, release from the membrane surface is significantly slower (15).

It is unclear whether the signal peptide binding interaction was broken at the point at which the FRET interaction was lost under transport conditions, or whether there is sufficient flexibility between the mature domain and signal peptide such that large movements of the mature domain away from the C termini of TatB and TatC can occur without dissociation of the signal peptide. The latter is consistent with the finding that the thylakoid Tat machinery can transport cargos covalently linked to TatC via their signal peptide (27). In contrast, the NADH-dependent release of the cargo from membranes containing

Downloaded from www.jbc.org at Texas A&M University - Medical Sciences Library, on April 2, 2012

TatBC complexes but no TatA (Fig. 5) indicates a weaker membrane binding affinity in the presence of a $\Delta\psi$ under these conditions, and thus clear dissociation of the signal peptide from the TatBC receptor complex under these conditions.

The analysis of the data in Fig. 2*D* indicates that the functional TatBC receptor concentration is $\leq\sim$20 nM (supplemental materials). Thus, the functional binding site concentration is significantly lower than the number of TatC molecules (322 ± 88 nM) calculated based on the mCherry concentration. Note that TatABC^{cherry} IMVs contained only full-length TatC^{cherry} (supplemental Fig. S11), indicating that the mCherry fluorescence signal was not contaminated by degradation products of the fusion protein. One possibility is that most TatC molecules are inaccessible or non-functional, possibly a consequence of overexpression. Tarry *et al.* (32) found that cargos bind to only a few available binding sites in TatBC oligomers, which they estimated to be heptamers. According to our data, active heptamers could account for ~140 nM ($=7 \times 20$ nM) of the TatC molecules present. The remaining ~180 nM of the TatC molecules present may then be inactive or inaccessible. However, a recent report with covalent TatC dimers suggests that TatBC complexes contain an even number of TatC molecules (40). Thus, the oligomerization state of active TatBC complexes remains uncertain.

For all the pre-SufI single cysteine mutants tested, FRET signals were higher with TatC^{cherry} than with TatB^{cherry}. This is seemingly at odds with a recent crosslinking study, which suggested that pre-SufI binds more closely to TatB than to TatC (28). However, the observed FRET signal arises from the proximity of the pre-SufI mature domain to the mCherry protein, which was at the C termini of the Tat proteins. Our data do not exclude the possibility that the dye molecules on the pre-SufI mutants are closer to the amphipathic region of TatB than to the TatB C terminus. Consequently, the models of Maurer *et al.* (28) are entirely consistent with our FRET data.

A model that has emerged for the *E. coli* Tat system and the pre-SufI cargo is that the cargo first binds to the membrane lipids. From there, the cargo laterally diffuses to the TatBC complex. Translocation across the membrane, presumably with the assistance of TatA oligomers, requires a $\Delta\psi$ (15). From studies on the thylakoid Tat system, the oligomerization of a TatBC complex with a TatA complex requires a PMF (41). It seems safe to deduce, then, that such an oligomerization process is responsible for the lag phase observed in Fig. 3*A*. Loss of FRET is fairly rapid after this lag phase, possibly indicating that migration of the cargo mature domain from TatBC is fairly quick after TatABC oligomerization is complete. Fig. 4*C* indicates that migration after binding occurs essentially immediately if the cargo is added ~200 s after $\Delta\psi$ generation has been initiated, possibly indicating that TatABC oligomerization occurred before the cargo bound to TatBC. The cargo migration away from TatBC is ~2.6-fold slower under these conditions, likely due to the fact that the detectable $\Delta\psi$ had already collapsed (Fig. 3*C*; see also Ref. 15) when the cargo was added. Receptor binding and migration of the mature domain away from the TatBC complex occurs concurrently in Fig. 4*C*. The absence of a detectable increase in FRET at the beginning part of the kinetics in Fig. 4*C* indicates a rapid binding step ($\tau \leq \sim$3 s), which includes both lipid binding and diffusion to the Tat translocon. Our data are therefore consistent with the hypothesis that TatBC and TatA oligomerization occurs in the presence of a $\Delta\psi$, with or without the cargo. Further, the $\Delta\psi$ makes the translocation system receptive to cargo movement from the receptor binding site (e.g. by a conformational change, or the oligomerization itself), but does not appear to directly drive it energetically. We expect that under *in vivo* conditions where a large $\Delta\psi$ is consistently maintained, all three Tat components can and do oligomerize and cargo transport occurs on the subminute timescale.

According to the oligomerization model discussed in the previous paragraph, TatA and TatBC form separate oligomers in the absence of a cargo and a PMF (8, 11, 40, 42). Thus, our expectation was that the stability of the TatBC-precursor complex should be unaffected by the absence of TatA in the presence or absence of a $\Delta\psi$. We were therefore surprised that pre-SufI was released from IMVs upon addition of NADH in the absence of TatA (Fig. 5*B*). We interpret these data to imply that the receptor complex has a weaker affinity for pre-SufI in the absence of TatA when a $\Delta\psi$ is present. This appears inconsistent with an oligomerization model in which TatA is not part of the receptor complex. However, an alternative, revised model is that at least some TatA is part of the receptor complex, consistent with earlier results (8, 42). This picture is also consistent with a recent study, which reports some cross-linking of pre-SufI to TatA in the absence of a PMF (43). In light of these data suggesting that TatA is part of the TatBC receptor complex, it is not at all surprising that the absence of TatA affects the interaction between TatBC and pre-SufI. According to our FRET assay, a weaker receptor complex binding affinity in the absence of TatA is only apparent in the presence of a PMF. TatA is necessary to keep pre-SufI bound to the TatBC complex in the presence of a PMF, eventually leading to transport (compare Figs. 4*A* and 5*A*).

In summary, we have isolated membranes exhibiting rapid Tat translocation activity. For TatABC^{cherry} IMVs, the overall translocation process is characterized by $\tau = \sim$80 s (Fig. 1*D*). When a $\Delta\psi$ is generated across these IMV membranes with bound precursor protein, migration away from the TatBC binding site occurs with $\tau = \sim$30 s after a significant (20–45 s) lag phase (Fig. 4*A*). Migration away from the TatBC binding site occurs more slowly, but with no lag phase, if the precursor is added to previously energized membranes ($\tau = \sim$90 s, Fig. 4*C*), suggesting that the effect of the $\Delta\psi$ slowly wears off or that transport in the presence of a weak, undetectable $\Delta\psi$ (15) occurs more slowly. Binding to the membrane surface and diffusion to the TatBC complex occurs rapidly ($\tau \leq \sim$3 s). Therefore, the migration process in which the cargo moves away from the TatBC complex requires a significant fraction (~40%) of the total transport time. It is unclear whether the migration step itself is rate-limiting or whether an upstream kinetic step limits the migration rate. The gel-based transport assay has poor time resolution, and, since it is not a real-time assay, it is not clear whether any transport substeps can occur after quenching the reaction. Consequently, it remains unclear whether the cargo proceeds directly across the membrane bilayer upon leaving the TatBC complex or whether there is an additional kinetically

Downloaded from www.jbc.org at Texas A&M University - Medical Sciences Library, on April 2, 2012

significant intermediate, *e.g.* cargo within the TatA pore. Further experiments are needed to clarify these downstream events.

Acknowledgments—We thank T. L. Yahr for pET-SufI and pTatABC, T. Palmer for MC4100 and MC4100ΔTatABCDE, and Anita Pokharel for technical assistance.

REFERENCES

1. Santini, C. L., Ize, B., Chanal, A., Müller, M., Giordano, G., and Wu, L. F. (1998) A novel sec-independent periplasmic protein translocation pathway in *Escherichia coli*. *EMBO J.* **17,** 101–112
2. Thomas, J. D., Daniel, R. A., Errington, J., and Robinson, C. (2001) Export of active green fluorescent protein to the periplasm by the twin-arginine translocase (Tat) pathway in *Escherichia coli*. *Mol. Microbiol.* **39,** 47–53
3. Sargent, F. (2007) The twin-arginine transport system: moving folded proteins across membranes. *Biochem. Soc. Trans.* **35,** 835–847
4. Natale, P., Brüser, T., and Driessen, A. J. (2008) Sec- and Tat-mediated protein secretion across the bacterial cytoplasmic membrane-distinct translocases and mechanisms. *Biochim. Biophys. Acta* **1778,** 1735–1756
5. Sargent, F., Bogsch, E. G., Stanley, N. R., Wexler, M., Robinson, C., Berks, B. C., and Palmer, T. (1998) Overlapping functions of components of a bacterial Sec-independent protein export pathway. *EMBO J.* **17,** 3640–3650
6. Sargent, F., Stanley, N. R., Berks, B. C., and Palmer, T. (1999) Sec-independent protein translocation in *Escherichia coli*. A distinct and pivotal role for the TatB protein. *J. Biol. Chem.* **274,** 36073–36082
7. Weiner, J. H., Bilous, P. T., Shaw, G. M., Lubitz, S. P., Frost, L., Thomas, G. H., Cole, J. A., and Turner, R. J. (1998) A novel and ubiquitous system for membrane targeting and secretion of cofactor-containing proteins. *Cell* **93,** 93–101
8. Bolhuis, A., Mathers, J. E., Thomas, J. D., Barrett, C. M., and Robinson, C. (2001) TatB and TatC form a functional and structural unit of the twin-arginine translocase from *Escherichia coli*. *J. Biol. Chem.* **276,** 20213–20219
9. Alami, M., Lüke, I., Deitermann, S., Eisner, G., Koch, H. G., Brunner, J., and Müller, M. (2003) Differential interactions between a twin-arginine signal peptide and its translocase in *Escherichia coli*. *Mol. Cell* **12,** 937–946
10. Jack, R. L., Sargent, F., Berks, B. C., Sawers, G., and Palmer, T. (2001) Constitutive expression of *Escherichia coli* tat genes indicates an important role for the twin-arginine translocase during aerobic and anaerobic growth. *J. Bacteriol.* **183,** 1801–1804
11. Gohlke, U., Pullan, L., McDevitt, C. A., Porcelli, I., de Leeuw, E., Palmer, T., Saibil, H. R., and Berks, B. C. (2005) The TatA component of the twin-arginine protein transport system forms channel complexes of variable diameter. *Proc. Natl. Acad. Sci. U.S.A.* **102,** 10482–10486
12. De Leeuw, E., Porcelli, I., Sargent, F., Palmer, T., and Berks, B. C. (2001) Membrane interactions and self-association of the TatA and TatB components of the twin-arginine translocation pathway. *FEBS Lett.* **506,** 143–148
13. Yahr, T. L., and Wickner, W. T. (2001) Functional reconstitution of bacterial Tat translocation *in vitro*. *EMBO J.* **20,** 2472–2479
14. Lüke, I., Handford, J. I., Palmer, T., and Sargent, F. (2009) Proteolytic processing of *Escherichia coli* twin-arginine signal peptides by LepB. *Arch. Microbiol.* **191,** 919–925
15. Bageshwar, U. K., Whitaker, N., Liang, F. C., and Musser, S. M. (2009) Interconvertibility of lipid- and translocon-bound forms of the bacterial Tat precursor pre-SufI. *Mol. Microbiol.* **74,** 209–226
16. Hou, B., Frielingsdorf, S., and Klösgen, R. B. (2006) Unassisted membrane insertion as the initial step in ΔpH/Tat-dependent protein transport. *J. Mol. Biol.* **355,** 957–967
17. Mould, R. M., and Robinson, C. (1991) A proton gradient is required for the transport of two lumenal oxygen-evolving proteins across the thylakoid membrane. *J. Biol. Chem.* **266,** 12189–12193
18. Cline, K., Ettinger, W. F., and Theg, S. M. (1992) Protein-specific energy requirements for protein transport across or into thylakoid membranes. Two lumenal proteins are transported in the absence of ATP. *J. Biol. Chem.* **267,** 2688–2696
19. Braun, N. A., Davis, A. W., and Theg, S. M. (2007) The chloroplast Tat pathway utilizes the transmembrane electric potential as an energy source. *Biophys. J.* **93,** 1993–1998
20. Bageshwar, U. K., and Musser, S. M. (2007) Two electrical potential-dependent steps are required for transport by the *Escherichia coli* Tat machinery. *J. Cell Biol.* **179,** 87–99
21. Berks, B. C., Palmer, T., and Sargent, F. (2003) The Tat protein translocation pathway and its role in microbial physiology. *Adv. Microb. Physiol.* **47,** 187–254
22. Bendtsen, J. D., Nielsen, H., Widdick, D., Palmer, T., and Brunak, S. (2005) Prediction of twin-arginine signal peptides. *BMC Bioinformatics* **6,** 167
23. Shanmugham, A., Wong Fong Sang, H. W., Bollen, Y. J., and Lill, H. (2006) Membrane binding of twin arginine preproteins as an early step in translocation. *Biochemistry* **45,** 2243–2249
24. Holzapfel, E., Eisner, G., Alami, M., Barrett, C. M., Buchanan, G., Lüke, I., Betton, J. M., Robinson, C., Palmer, T., Moser, M., and Müller, M. (2007) The entire N-terminal half of TatC is involved in twin-arginine precursor binding. *Biochemistry* **46,** 2892–2898
25. Kreutzenbeck, P., Kröger, C., Lausberg, F., Blaudeck, N., Sprenger, G. A., and Freudl, R. (2007) *Escherichia coli* twin arginine (Tat) mutant translocases possessing relaxed signal peptide recognition specificities. *J. Biol. Chem.* **282,** 7903–7911
26. Strauch, E. M., and Georgiou, G. (2007) *Escherichia coli* tatC mutations that suppress defective twin-arginine transporter signal peptides. *J. Mol. Biol.* **374,** 283–291
27. Gérard, F., and Cline, K. (2006) Efficient twin arginine translocation (Tat) pathway transport of a precursor protein covalently anchored to its initial cpTatC binding site. *J. Biol. Chem.* **281,** 6130–6135
28. Maurer, C., Panahandeh, S., Jungkamp, A. C., Moser, M., and Müller, M. (2010) TatB functions as an oligomeric binding site for folded Tat precursor proteins. *Mol. Biol. Cell* **21,** 4151–4161
29. Gérard, F., and Cline, K. (2007) The thylakoid proton gradient promotes an advanced stage of signal peptide binding deep within the Tat pathway receptor complex. *J. Biol. Chem.* **282,** 5263–5272
30. Frielingsdorf, S., and Klösgen, R. B. (2007) Prerequisites for terminal processing of thylakoidal Tat substrates. *J. Biol. Chem.* **282,** 24455–24462
31. Schlesier, R., and Klösgen, R. B. (2010) Twin arginine translocation (Tat)-dependent protein transport: the passenger protein participates in the initial membrane binding step. *Biol. Chem.* **391,** 1411–1417
32. Tarry, M. J., Schäfer, E., Chen, S., Buchanan, G., Greene, N. P., Lea, S. M., Palmer, T., Saibil, H. R., and Berks, B. C. (2009) Structural analysis of substrate binding by the TatBC component of the twin-arginine protein transport system. *Proc. Natl. Acad. Sci. U.S.A.* **106,** 13284–13289
33. Wexler, M., Sargent, F., Jack, R. L., Stanley, N. R., Bogsch, E. G., Robinson, C., Berks, B. C., and Palmer, T. (2000) TatD is a cytoplasmic protein with DNase activity. No requirement for TatD family proteins in sec-independent protein export. *J. Biol. Chem.* **275,** 16717–16722
34. Casadaban, M. J., and Cohen, S. N. (1979) Lactose genes fused to exogenous promoters in one step using a Mu-lac bacteriophage: *in vivo* probe for transcriptional control sequences. *Proc. Natl. Acad. Sci. U.S.A.* **76,** 4530–4533
35. Studier, F. W., Rosenberg, A. H., Dunn, J. J., and Dubendorff, J. W. (1990) Use of T7 RNA polymerase to direct expression of cloned genes. *Methods Enzymol.* **185,** 60–89
36. Yanisch-Perron, C., Vieira, J., and Messing, J. (1985) Improved M13 phage cloning vectors and host strains: nucleotide sequences of the M13mp18 and pUC19 vectors. *Gene* **33,** 103–119
37. Chong, S., Montello, G. E., Zhang, A., Cantor, E. J., Liao, W., Xu, M. Q., and Benner, J. (1998) Utilizing the C-terminal cleavage activity of a protein splicing element to purify recombinant proteins in a single chromatographic step. *Nucleic Acids Res.* **26,** 5109–5115
38. Shaner, N. C., Campbell, R. E., Steinbach, P. A., Giepmans, B. N., Palmer, A. E., and Tsien, R. Y. (2004) Improved monomeric red, orange, and yellow fluorescent proteins derived from Discosoma sp. red fluorescent protein. *Nat. Biotechnol.* **22,** 1567–1572
39. Panahandeh, S., Maurer, C., Moser, M., DeLisa, M. P., and Müller, M.

Downloaded from www.jbc.org at Texas A&M University - Medical Sciences Library, on April 2, 2012

(2008) Following the path of a twin-arginine precursor along the TatABC translocase of Escherichia coli. *J. Biol. Chem.* **283,** 33267–33275
40. Maldonado, B., Buchanan, G., Müller, M., Berks, B. C., and Palmer, T. (2011) Genetic evidence for a TatC dimer at the core of the *Escherichia coli* twin arginine (Tat) protein translocase. *J. Mol. Microbiol. Biotechnol.* **20,** 168–175
41. Mori, H., and Cline, K. (2002) A twin arginine signal peptide and the pH gradient trigger reversible assembly of the thylakoid ΔpH/Tat translocase. *J. Cell Biol.* **157,** 205–210
42. de Leeuw, E., Granjon, T., Porcelli, I., Alami, M., Carr, S. B., Müller, M., Sargent, F., Palmer, T., and Berks, B. C. (2002) Oligomeric properties and signal peptide binding by *Escherichia coli* Tat protein transport complexes. *J. Mol. Biol.* **322,** 1135–1146
43. Fröbel, J., Rose, P., and Müller, M. (2011) Early contacts between substrate proteins and TatA translocase component in twin-arginine translocation. *J. Biol. Chem.* **286,** 43679–43689

Downloaded from www.jbc.org at Texas A&M University - Medical Sciences Library, on April 2, 2012

Derivation of the Binding Equation Including the Receptor Concentration (Equation 2 for Figure 2D)

If it can be assumed that the TatBC complex concentration is much less than the precursor K_D, the binding data in Figure 2D can be fit to a typical single site binding equation:

$$y = \frac{B_{max} x}{(K_D + x)} \qquad \text{(equation 3)}$$

However, if the TatBC concentration and K_D are of similar magnitude, this equation is invalid. The appropriate fitting equation is derived as follows.

The relevant binding equilibrium is:

$$P + T \underset{k_{-1}}{\overset{k_1}{\rightleftharpoons}} PT \qquad K_D = \frac{k_{-1}}{k_1} = \frac{[P][T]}{[PT]} \qquad \text{(equation 4)}$$

where P is the precursor and T is the Tat(A)BC receptor complex. Assuming that P_a is the total amount of precursor added and that T_0 is the concentration of receptor binding sites, mass balance yields:

$$P_a = [P] + [PT]$$

$$T_0 = [T] + [PT]$$

[PT] can then be obtained from equation 4 after substitution and use of the quadratic formula,

$$K_D[PT] = [P][T]$$

$$K_D[PT] = \left(P_a - [PT]\right)\left(T_0 - [PT]\right)$$

$$0 = [PT]^2 - (P_a + T_0 + K_D)[PT] + P_a T_0$$

$$[PT] = \frac{(P_a + T_0 + K_D) \pm \sqrt{(P_a + T_0 + K_D)^2 - 4P_a T_0}}{2}$$

The proper solution is given by the difference in the numerator. Since T_0 is unknown, dividing by T_0 yields the percent occupancy of the available binding sites,

$$\frac{[PT]}{T_0} = \frac{(P_a + T_0 + K_D) - \sqrt{(P_a + T_0 + K_D)^2 - 4P_a T_0}}{2T_0} \qquad \text{(equation 5)}$$

A multiplicative scaling factor, C, was then used to fit the data in Figure 2D with C, T_0 and K_D as fitting parameters,

$$y = C * \frac{(x + T_0 + K_D) - \sqrt{(x + T_0 + K_D)^2 - 4(x)T_0}}{2T_0} \qquad \text{(equation 6)}$$

Equation 6 is the formula given in the Experimental Procedures section (equation 2).

Note that if $T_0 << K_D$, then [P] can be approximated by P_a (i.e., the bound precursor is always a small fraction of the total precursor added). Under these conditions,

Downloaded from www.jbc.org at Texas A&M University - Medical Sciences Library, on April 2, 2012

$$K_D \approx \frac{P_a(T_0 - [PT])}{[PT]}$$

or,

$$\frac{[PT]}{T_0} \approx \frac{P_a}{K_D + P_a} \qquad \text{(equation 7)}$$

With the exception of a scaling factor, equation 7 is identical to equation 3.

Unfortunately, fitting the data in Figure 2D with equation 6 does not yield a robust, unique solution for T_0 and K_D. However a range of possible values can be determined by determining the extremes of possible values. In principle, T_0 could be infinitely small. However, the K_D determined from the fit is essentially identical (= 23 nM) for $T_0 \leq 0.1$ nM. For T_0 = 20 nM, the K_D = 7.5 nM. For T_0 > 20 nM, the fit becomes significantly worse. Thus, a range of possible values consistent with the data in Figure 2D is $T_0 \approx$ 0-20 nM, and $K_D \approx$ 7-23 nM. Due to the high mCherry concentration present in our samples, which reports on the receptor concentration, a high T_0 (~20 nM) is more likely, which corresponds to the lower end of the K_D range (i.e., ~7 nM).

Downloaded from www.jbc.org at Texas A&M University - Medical Sciences Library, on April 2, 2012

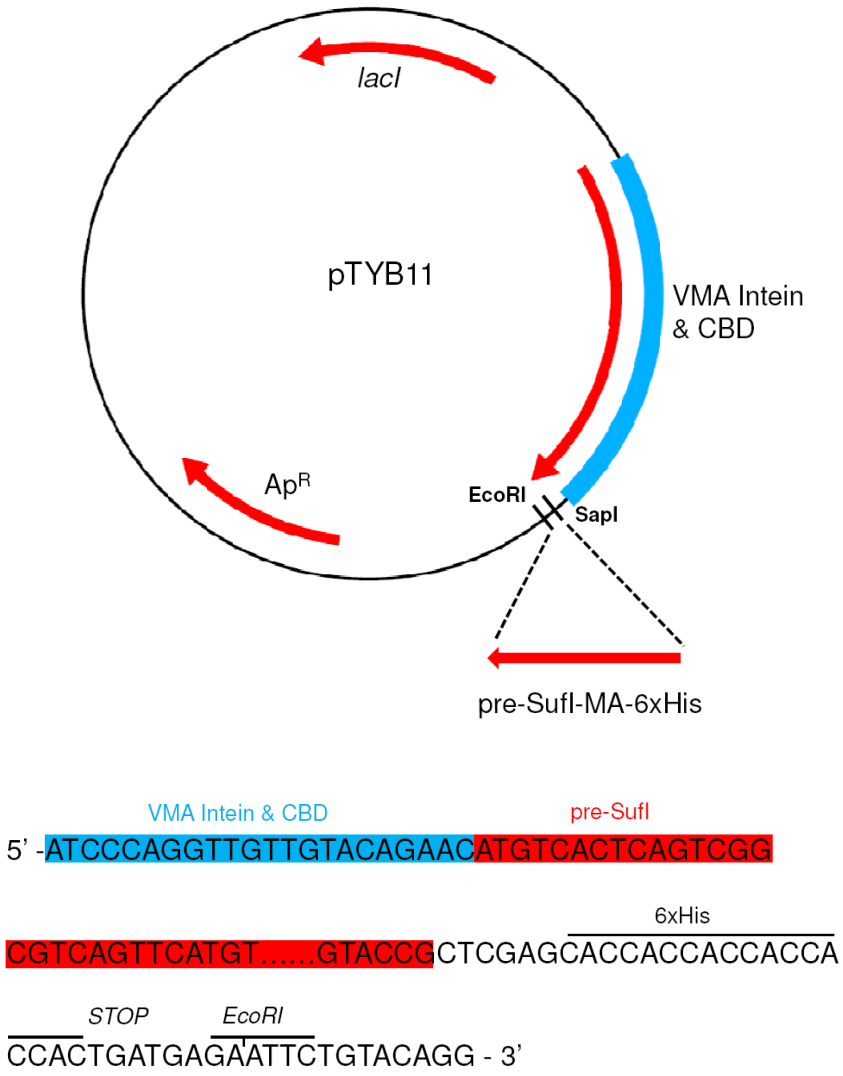

Figure S1. Generation of pIntein-preSufI-MA from pTYB11. The plasmid pIntein-preSufI-MA was generated by inserting a cysteine-free form of pre-SufI with a 6xHis tag into the vector pTYB11 (New England Biolabs) at restriction enzyme sites SapI and EcoRI. Since SapI does not cleave at the restriction enzyme recognition site, the recognition sequence was lost after insertion of the pre-SufI sequence. The pre-SufI gene was obtained from pET-SufI (13) and the cysteines were removed with mutations C17M and C295A. Site directed mutagenesis was used to generate plasmids pIntein-preSufI-MA(G29C), pIntein-preSufI-MA(G45C), pIntein-preSufI-MA(T96C), pIntein-preSufI-MA(S204C), pIntein-preSufI-MA(M338C), pIntein-preSufI-MA(G410C), the names of which reflect single cysteine mutations in the mature region of the pre-SufI protein. Plasmids pIntein-preSufI-MA(L470C) and pIntein-preSufI-MA(479C) were made by mutating a leucine in the short linker region between the mature domain and the 6xHis tag (CTC codon), and by adding a cysteine residue to the C-terminus, respectively.

Downloaded from www.jbc.org at Texas A&M University - Medical Sciences Library, on April 2, 2012

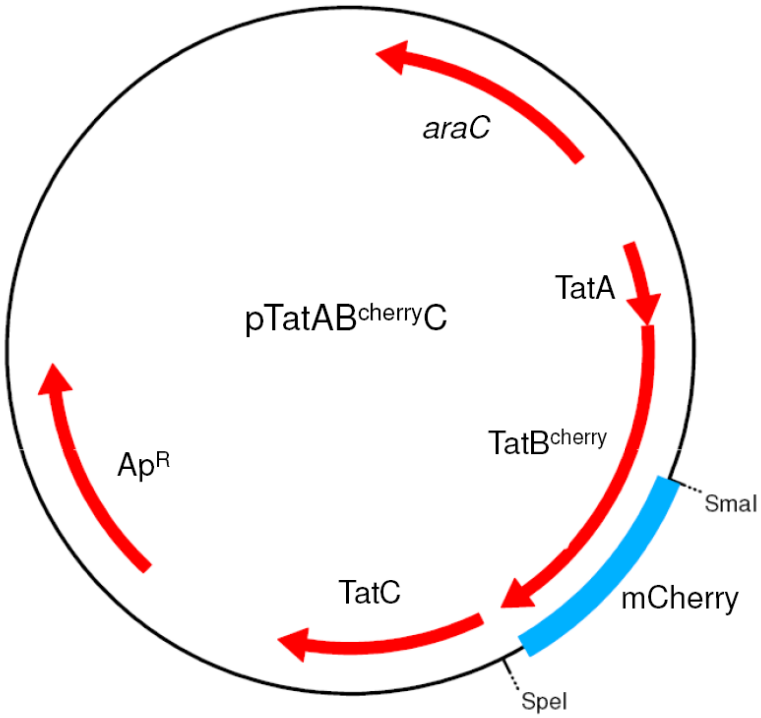

TatB SmaI mCherry

5’ -CCGTATACCCGGGTACCGGTCGCCACCATGGTG……

STOP

TACAAGTAGCGGCCGCGACTCTAGAATTCCAACTGAGCGC

CGGTCGCTACCATTACCAACTTGTCTGGTGTCAAAAA

SpeI TatC

TAATAGGCCTACTAGTCATGTCT- 3’

Figure S2. Plasmid map of pTatAB^{cherry}C. Plasmid pTatAB^{cherry}C was generated by insertion of the mCherry sequence (plasmid pmCherry, Clontech) between restriction sites SmaI and SpeI. These restriction sites were inserted into pTatABC (13) immediately after the coding region of TatB by site-directed mutagenesis, as indicated, deleting the stop codon.

Downloaded from www.jbc.org at Texas A&M University - Medical Sciences Library, on April 2, 2012

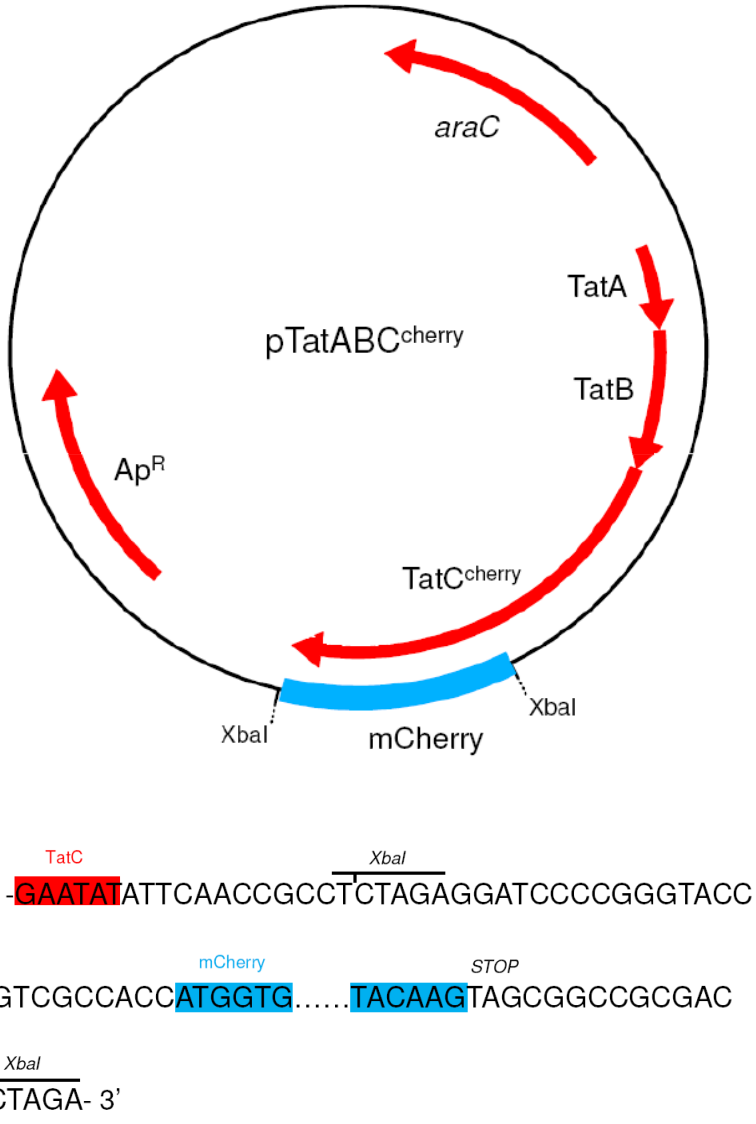

Figure S3. Plasmid map of pTatABC^{cherry}. Plasmid pTatABC^{cherry} was generated by insertion of the mCherry sequence into pTatABC immediately after the coding region of TatC by insertion at an XbaI site. The TatC stop codon was removed by site-directed mutagenesis.

Downloaded from www.jbc.org at Texas A&M University - Medical Sciences Library, on April 2, 2012

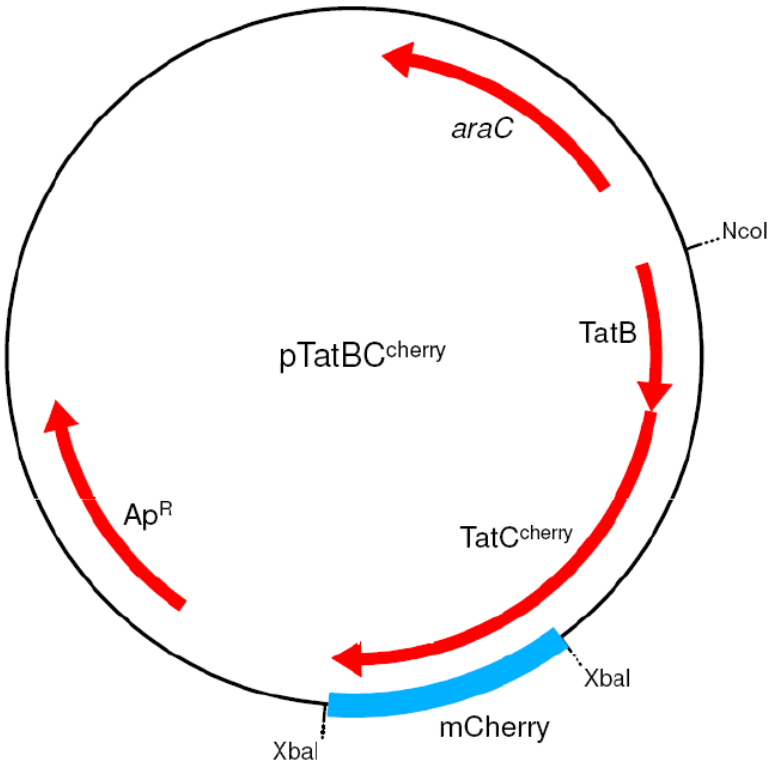

Figure S4. Plasmid map of pTatBC^{cherry}. Plasmids pTatBC and pTatBC^{cherry} were generated by engineering two NcoI sites flanking the TatA coding sequence and excising *tatA* from pTatABC and pTatABC^{cherry}, respectively.

Downloaded from www.jbc.org at Texas A&M University - Medical Sciences Library, on April 2, 2012

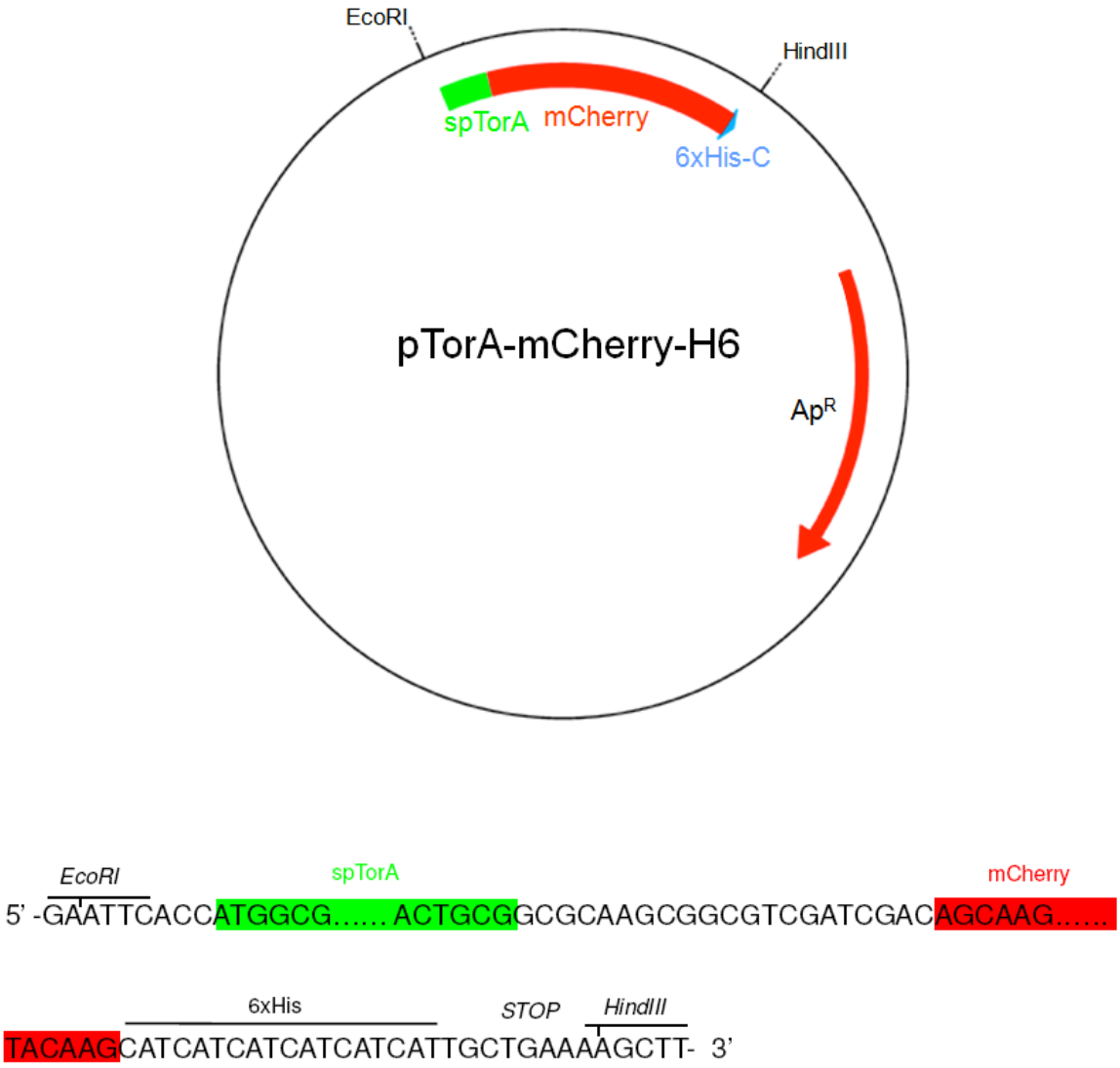

Figure S5. Plasmid map of pTorA-mCherry-H6. The coding sequence for the TorA signal peptide (from plasmid pTorA-GFP (20)) was fused with the coding sequence for mCherry, as indicated, between restriction sites EcoRI and HindIII of pBAD24 (ATCC). The first four amino acids following spTorA (AQAA) are from the N-terminus of the TorA mature domain.

Downloaded from www.jbc.org at Texas A&M University - Medical Sciences Library, on April 2, 2012

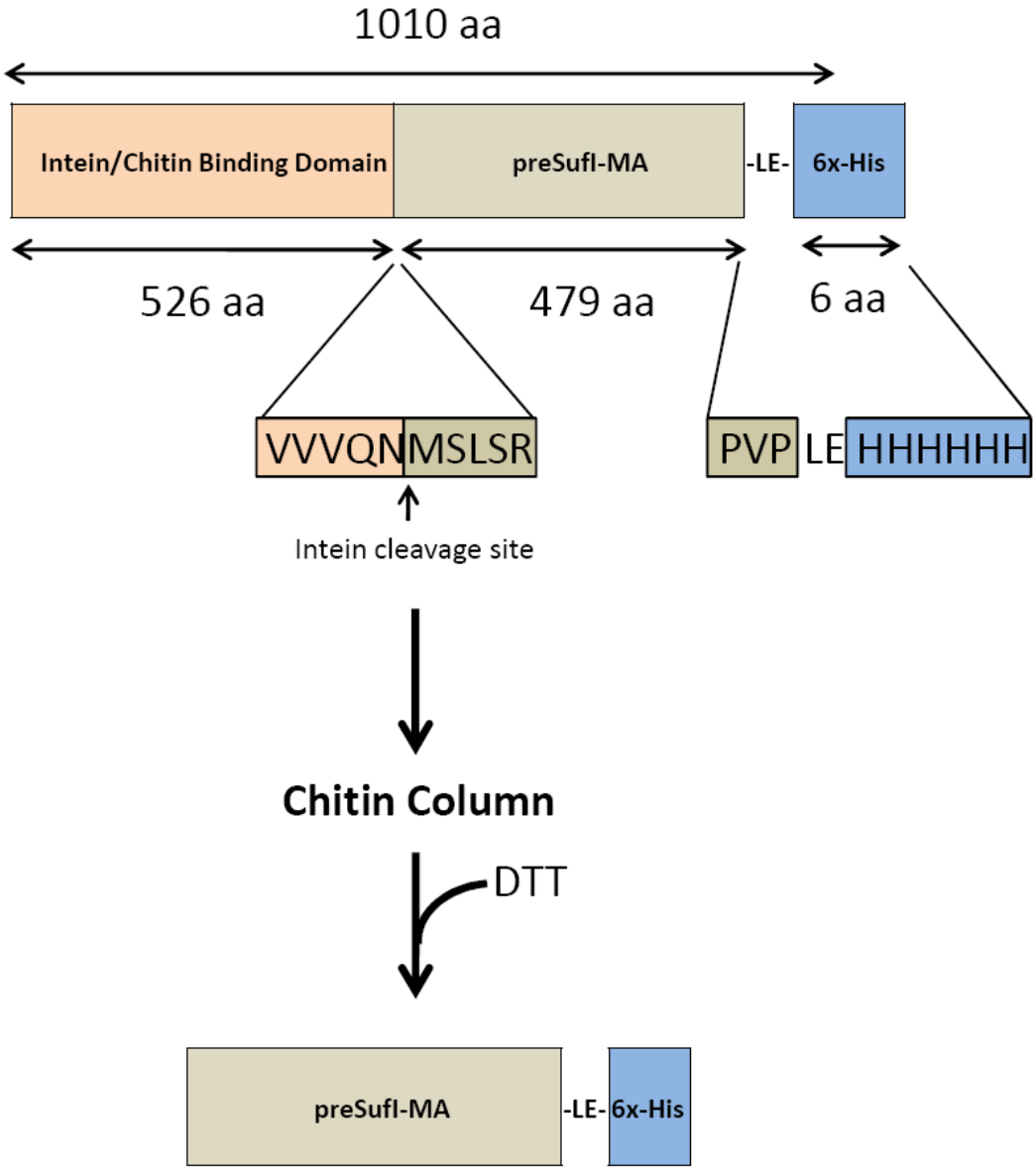

Figure S6. Purification of pre-SufI. In order to obtain pure precursor protein free from mature protein, pre-SufI was purified using the IMPACT-CN system according to the manufacturer (New England Biolabs). In brief, a bifunctional tag, consisting of intein and chitin binding domains, was fused to the N-terminus of pre-SufI. Crude cell extracts were added directly to a chitin column. Pre-SufI was cleaved off the column by activating intein cleavage by the addition of DTT. The protein was further purified by Ni-NTA chromatography, as described (20).

Downloaded from www.jbc.org at Texas A&M University - Medical Sciences Library, on April 2, 2012

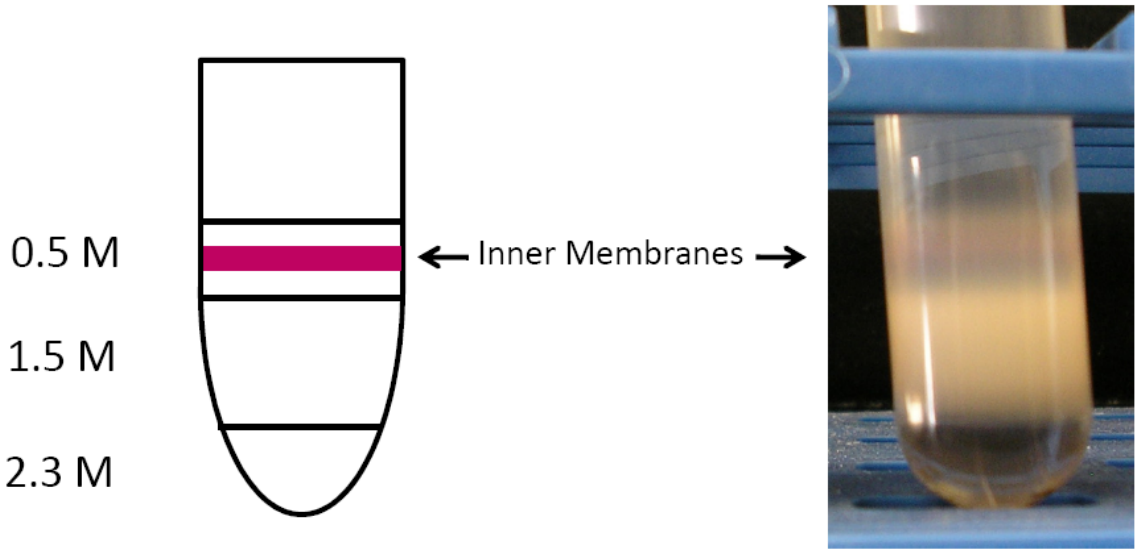

Figure S7. Sucrose gradient for IMV isolation. A three step (0.5 M, 1.5 M, and 2.3 M) sucrose gradient was used for IMV purification in Buffer B (1 mM KCl, 1 mM $MgSO_4$, 2 mM DTT, 10 mM Hepes, pH 7.0) (20). IMVs typically sedimented within the 0.5 M sucrose fraction. A sucrose gradient with membranes containing $TatABC^{cherry}$ is shown on the right. We previously reported that IMV preparations with *E. coli* strain JM109 consistently yielded high transport efficiencies, but attempts with strain MC4100 were less successful, for unknown reasons (20). The Tat proteins in this study were all expressed in strain MC4100ΔTatABCDE in order to obtain IMVs in which all TatB or TatC molecules were labeled with mCherry. The pink color of proteins labeled with mCherry served as a convenient marker during purification of inner membranes on a sucrose gradient as shown. Consequently, the recovered membranes were significantly more highly purified. Moreover, the IMVs displayed more consistent transport activity both in terms of transport efficiencies and transport rate. Transport rates were about an order of magnitude faster (Fig. 1*D*) than reported earlier (15,20). We expect that this is a consequence of the higher purity of the IMV preparations.

Downloaded from www.jbc.org at Texas A&M University - Medical Sciences Library, on April 2, 2012

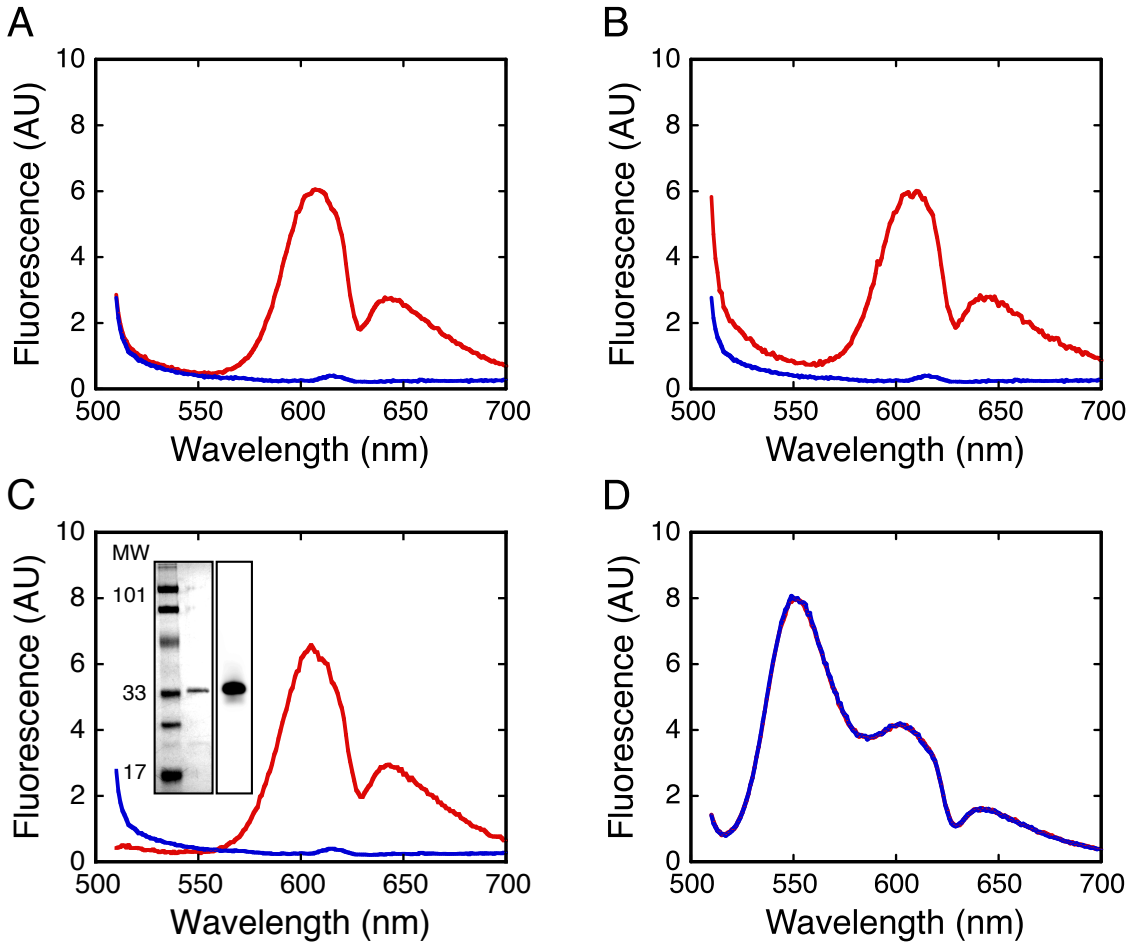

Figure S8. Fluorescence emission of mCherry-tagged proteins and lack of FRET for non-interacting proteins. (A and B) Emission spectra of IMVs containing TatAB^{cherry}C (A, *red*), TatABC^{cherry} (B, *red*) and TatABC (*blue*). (C) Emission spectra of mCherry (*red*) and TatABC IMVs (*blue*). Note that the mCherry protein exhibits two emission peaks. The mCherry protein was obtained by combining fractions of mature-length protein obtained from anion-exchange chromatography of spTorA-mCherry-H6. (inset, left) Coomassie blue stained SDS-PAGE gel of mCherry, with molecular weight ladder in the left lane. (inset, right) Fluorescence of the same gel before staining. The native structure of mCherry is retained on this gel because the sample was not boiled. As further tests to identify the reason behind the two well-resolved peaks for mCherry in our experiments, we tested phosphate buffer (eliminating effects of a component in the transport buffer), excitation wavelength (eliminating an off-peak excitation effect), and slit width (eliminating resolution due to a narrow emission window). None of these different conditions eliminated the two well-resolved peaks for mCherry emission. (D) Emission spectra of a mixture of pre-SufI(T96C)^{Alexa532} (20 nM) and spTorA-mCherry (300 nM) before (*red*) and after (*blue*) addition of 200 nM unlabeled pre-SufI(T96C). Note that there is no difference in the intensities of any of the peaks (compare with Fig. 2*A*). This confirms that the increase in the 550 nm peak observed in Fig. 2*A* results from loss of FRET. EX = 500 nm for all spectra.

Downloaded from www.jbc.org at Texas A&M University - Medical Sciences Library, on April 2, 2012

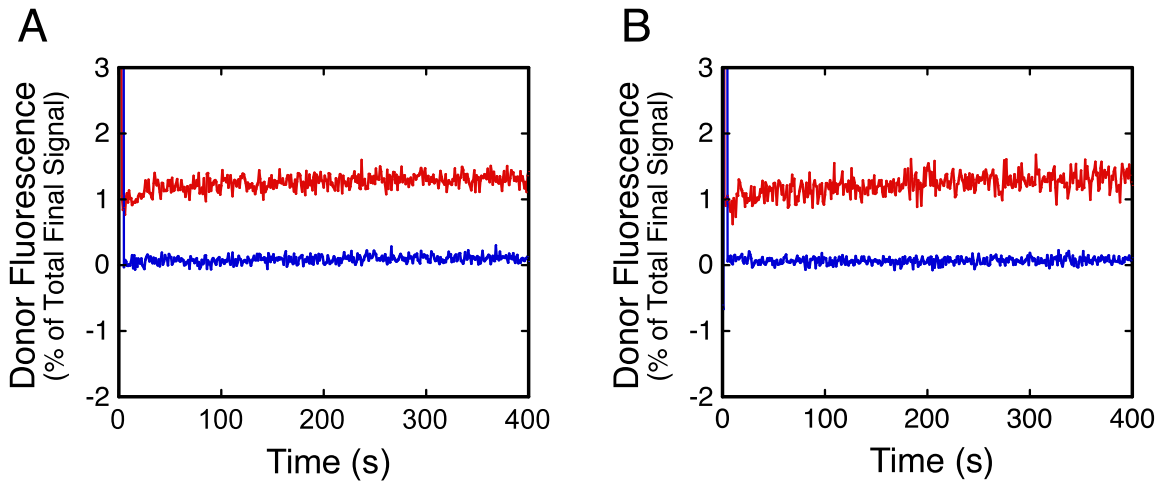

Figure S9. Control experiments for FRET kinetics. (A) Donor emission at 550 nm (EX = 500 nm) after addition of 200 nM unlabeled pre-SufI(T96C) at *t* = 0 s. Conditions are as in Fig. 2B except with TatABC IMVs (*red*) (i.e., with no mCherry acceptor) or with unlabeled pre-SufI(T96C) (*blue*) (i.e., with no Alexa532 donor). These data indicate that no observable signal change was detectable without both donor and acceptor fluorophores (compare with Fig. 2*B*). (B) Same as (A) except that reactions were initiated with 4 mM NADH at *t* = 0 s instead of competitor. Again, no observable signal change was detectable without both donor and acceptor fluorophores (compare with Fig. 4). For both panels, the same ordinate scale was used as in Figs. 2*B* and 4. Traces were zeroed and the upper traces (*red*) were displaced for clarity.

Downloaded from www.jbc.org at Texas A&M University - Medical Sciences Library, on April 2, 2012

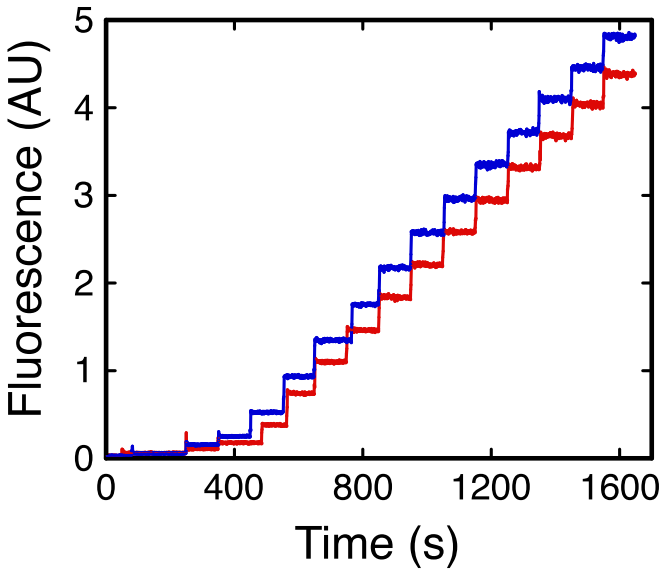

Figure S10. Titrations used to determine binding affinity. Sample titration of TatABC^{cherry} IMVs with pre-SufI(T96C)^{Alexa532} in the presence (*blue*) and absence (*red*) of 300 nM pre-SufI(T96C) as a competitive inhibitor. Each step results from the addition of pre-SufI(T96C)^{Alexa532}. One of the data sets used to generate Fig. 2*D*. EX = 500 nm; EM = 550 nm.

Downloaded from www.jbc.org at Texas A&M University - Medical Sciences Library, on April 2, 2012

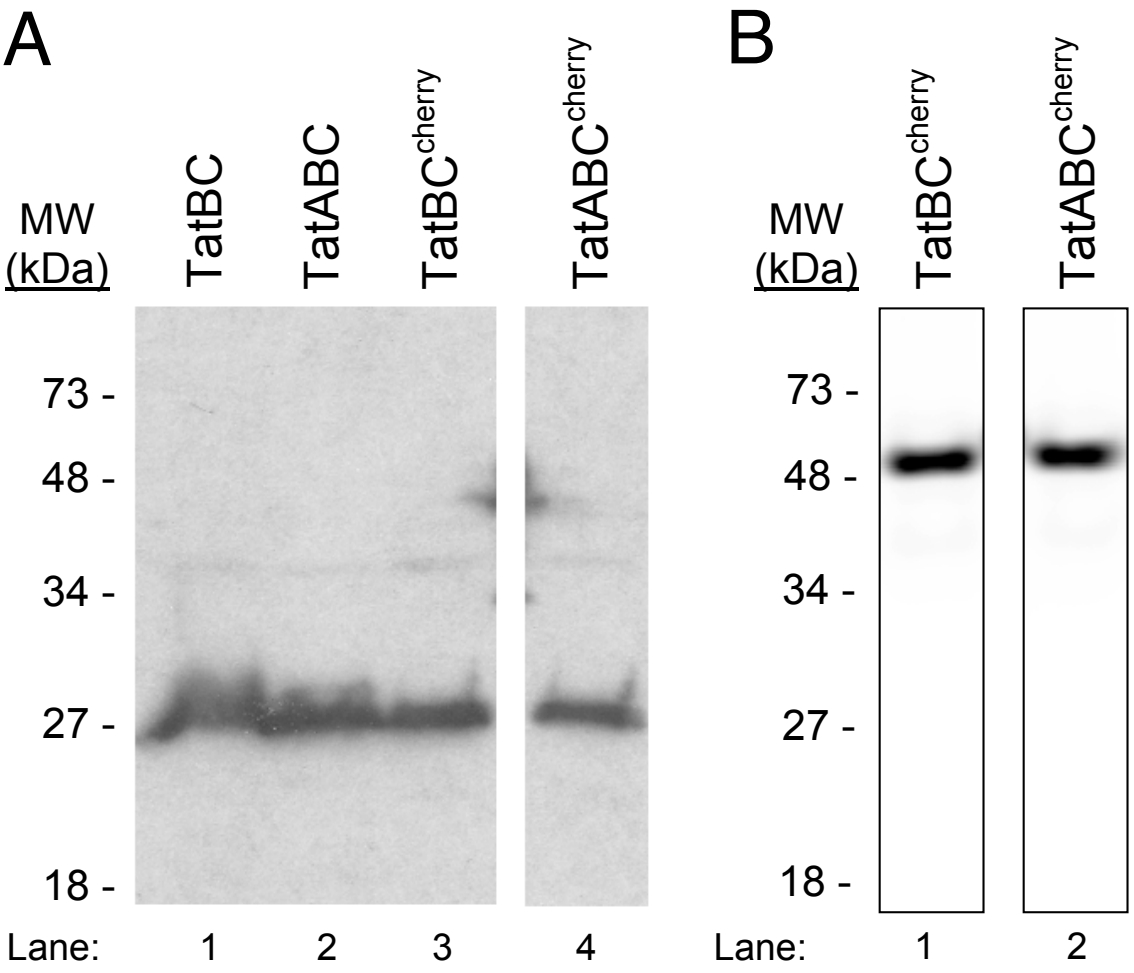

Figure S11. Expression of Tat proteins. (A) Western blot of the indicated IMV preparations using TatB antibodies. TatB protein levels are approximately the same in IMVs with or without TatA. The SDS-PAGE gel was electroblotted onto PVDF membranes and immunoblotted with rabbit polyclonal TatB antibodies (13) (1:5,000 dilution in 2% nonfat dry milk, 0.1% Triton X-100, and 0.1% Tween). Goat polyclonal anti–rabbit IgG-HRP conjugate (1:15,000; Santa Cruz Biotechnology, Inc.) was used as the secondary antibody, and bands were visualized by chemiluminescence. (B) $TatC^{cherry}$ fusions in the indicated IMV prreparations visualized by mCherry fluorescence. These data indicate that the mCherry protein was only present as part of the full-length fusion protein. The predicted molecular weights of TatB, TatC and $TatC^{cherry}$ are 18, 29, and 57 kDa, respectively. Note, however, that TatB and TatC migrate abnormally on gels (5).

Downloaded from www.jbc.org at Texas A&M University - Medical Sciences Library, on April 2, 2012